A Nebulin Ruler Does Not Dictate Thin Filament Lengths

Angelica Castillo,[†] Roberta Nowak,[‡] Kimberly P. Littlefield,[§] Velia M. Fowler,[‡] and Ryan S. Littlefield[§*]
[†]Department of Forensic Science, Chaminade University, Honolulu, Hawaii [‡]Department of Cell Biology, The Scripps Research Institute, La Jolla, California; and [§]Center for Cell Dynamics, University of Washington, Friday Harbor Laboratories, Friday Harbor, Washington

ABSTRACT To generate force, striated muscle requires overlap between uniform-length actin and myosin filaments. The hypothesis that a nebulin ruler mechanism specifies thin filament lengths by targeting where tropomodulin (Tmod) caps the slow-growing, pointed end has not been rigorously tested. Using fluorescent microscopy and quantitative image analysis, we found that nebulin extended 1.01–1.03 μm from the Z-line, but Tmod localized 1.13–1.31 μm from the Z-line, in seven different rabbit skeletal muscles. Because nebulin does not extend to the thin filament pointed ends, it can neither target Tmod capping nor specify thin filament lengths. We found instead a strong correspondence between thin filament lengths and titin isoform sizes for each muscle. Our results suggest the existence of a mechanism whereby nebulin specifies the minimum thin filament length and sarcomere length regulates and coordinates pointed-end dynamics to maintain the relative overlap of the thin and thick filaments during myofibril assembly.

INTRODUCTION

Actin filament lengths are precisely regulated to produce specialized cellular structures such as cochlear stereocilia, intestinal microvilli, and striated muscle myofibrils. In vertebrate striated myofibrils, the giant protein nebulin is thought to specify the diverse actin (thin) filament length distributions found in different muscles through a molecular ruler mechanism (1–5). Using this mechanism, the sarcomeric location of nebulin's N-terminal domain specifies the position of its binding partner, tropomodulin (Tmod) (6), which caps and regulates the dynamics of the thin filament slow-growing, pointed ends (P-ends) (7–10). In support of this mechanism, nebulin coextends along the thin filament up to ~1 μm from the Z-line (6,11–13), and nebulin's size (600–900 kDa) correlates with thin filament lengths in different species (1,14). Thus, variations in nebulin size by alternative splicing (15,16) are thought to generate diverse thin filament lengths in different skeletal muscles (4,17), allowing them to function in a variety of physiological contexts.

However, some studies have suggested that nebulin is not required, and that a ruler mechanism is not used, to specify thin filament lengths in some muscle types. For example, the thin filaments in *Drosophila* indirect flight muscle do not contain nebulin, but they are extremely uniform in length and gradually elongate from their P-ends during sarcomere growth (18), thereby maintaining full overlap with the thick filaments (19). Additionally, in vertebrate cardiac muscle, the thin filaments—which have broad, but nonrandom and distinct, length distributions in atria and ventricles (20) —contain nebulette, a small homolog of nebulin that is unable to extend fully along the lengths of the cardiac thin filaments (21), and only substoichiometric amounts of full-length nebulin (3). Although the presence of a modified nebulin ruler mechanism for cardiac muscle has been proposed (2), nebulin knockout mice have shown no defects in cardiac structure or function (22,23), suggesting that nebulin does not regulate cardiac thin filament lengths. Finally, in nebulin knockout mice, skeletal muscle thin filaments had uniform lengths at birth, revealing the presence of a nebulin-independent mechanism of length regulation (22). However, the thin filament lengths were shorter, exhibited reduced muscle-specific variations, and became progressively nonuniform after birth, indicating that nebulin has a significant role in regulating and maintaining lengths of skeletal muscle thin filaments (22,23). Therefore, many important questions remain unanswered by these studies: How does nebulin contribute to specifying diverse thin filament lengths in different muscles? And what is the nature of these nebulin-independent mechanisms for specifying thin filament lengths in these different systems? For example, does the nebulin-independent mechanism in skeletal muscle specify thin filament lengths when nebulin is normally present or, as suggested by Bang et al. (22), does a nebulin ruler mechanism take priority over the nebulin-independent mechanism?

To address these questions, we examined whether the N-terminal Tmod-binding domain of nebulin is located in the correct position to regulate P-end capping and to specify thin filament lengths through a ruler mechanism. In particular, does the N-terminal Tmod-binding domain of nebulin precisely colocalize with Tmod at the extreme P-end of the thin filament as predicted by the nebulin ruler mechanism (4,6,17,24)? To test this, we used indirect immunofluorescence and distributed deconvolution image analysis (5) to accurately localize the N-terminal end of nebulin and Tmod within myofibrils from seven previously characterized rabbit muscles (1,11,12,25–28). Similar to conventional deconvolution microscopy (29) and single-molecule methods (30), distributed deconvolution image analysis uses the entire distribution of fluorescence intensities to precisely determine

Submitted September 21, 2008, and accepted for publication October 28, 2008.

*Correspondence: ryanccd@u.washington.edu

Editor: Malcolm Irving.

0006-3495/09/03/1856/10 $2.00

doi: 10.1016/j.bpj.2008.10.053

the positions of regular striations within myofibrils at super-resolution (5). We exploited the natural variation of nebulin isoform sizes within these muscles to further determine whether nebulin isoforms specify different thin filament lengths in different muscle types within a single species. Our results showed that thin filament P-ends marked by the location of Tmod extended significantly beyond nebulin's N-terminal end by 0.1–0.3 μm in all seven muscles, indicating that nebulin does not extend to the thin filament P-end. We also found that average thin filament lengths in the different muscles were not accounted for by nebulin isoform size, but, instead, the lengths strongly correlated with titin isoform size. Our measurements were consistent with a novel mechanism, whereby nebulin sets the minimum thin filament length and P-end dynamics are regulated to increase thin filament lengths and optimize thin-thick filament overlap.

MATERIALS AND METHODS

Reagents and antibodies

All chemicals were purchased from Sigma (St. Louis, MO), unless otherwise indicated. Antibodies and fluorescent phalloidins were characterized for optimal dilutions. Alexa Fluor 488 phalloidin and Alexa Fluor 568 phalloidin (Molecular Probes, Eugene, OR) were used at 1:100–1:400 dilution. Sarcomeric α-actinin monoclonal antibody EA-53 was used at 1:1000–1:4000; affinity purified rabbit antibodies to human tropomodulin (rabbit 1749) were used at 3–5 μg/mL. The NebN antibody (rabbit 1357L, a generous gift from Dr. Carol Gregorio, University of Arizona, Tucson, AZ) was used at 1:100–1:500. The NebN epitope observed in these rabbit muscles is likely to correspond to the extreme N-terminal region (which the antibody was raised against), because this region is highly conserved between rabbit, mouse, rat, and human nebulin (see Fig. S1 *A* in the Supporting Material) and distinct from other regions of the nebulin molecule (6,16). Myofibril staining was not observed in the absence of the NebN or Tmod antibody (A. Castillo, R. Nowak, V. M. Fowler, and R. S. Littlefield, unpublished results). Secondary antibodies (Jackson ImmunoResearch, West Grove, PA) were used at the recommended 1:200 dilution.

Rabbit and chicken tissue

Rabbit muscle strips (2–4 cm) were isolated from adult male, New Zealand white, rabbits (R&R Rabbitry, Stanwood, WA; USDA license no. 91-R-0038. Euthanasia approved by AWA no. A3982-01). Chicken biventer muscles were isolated from local farm-raised hens. Muscle strips were stretched, tied to plastic syringe plungers, and stored overnight at 4°C in EGTA-Ringer's relaxing buffer (100 mM NaCl, 2 mM KCl, 2 mM $MgCl_2$, 6 mM potassium phosphate, 1 mM EGTA, 0.1% glucose, pH 7.0 at 0°C). Relaxed muscle strips were transferred to rigor buffer (100 mM KCl, 2 mM $MgCl_2$, 1 mM EDTA, 1 mM dithiothreitol, 10 mM potassium phosphate, pH 7.0 at 0°C) containing 50% glycerol and stored at −20°C. Fresh rigor buffer with 50% glycerol was exchanged the next day. All solutions contained Complete protease inhibitors (Roche Molecular Biochemicals, Indianapolis, IN). Myofibrils were prepared from muscle after at least 2 days of extraction.

For cryosectioning, relaxed rabbit muscle strips were fixed overnight at 4°C in fresh 4% paraformaldehyde (EM Sciences, Hatfield, PA) in phosphate buffered saline (PBS) containing 1 mM EGTA, cut into small blocks, infused with 20% sucrose overnight at 4°C, and embedded in Tissue-Tek OCT compound (EM Sciences). Cryosections (7–11 μm) were cut using a Reichert-Jung Cryomicrotome 800 cryostat (Leica, Nussloch, Germany), transferred onto glass slides, and stored at −20°C.

For Triton-extracted myofibrils, relaxed rabbit muscle strips were transferred to rigor buffer containing 1% Triton X-100 (Sigma) and stored overnight at 4°C, followed by myofibril isolation.

Myofibril isolation

Isolated myofibrils were prepared as described previously (5). Briefly, to ensure that stretched myofibrils were isolated, the central portion of a glycerinated (or Triton-extracted) muscle strip was minced in 10–15 mL of fresh rigor buffer containing protease inhibitors and mechanically homogenized with a Tempest Virtishear (VirTis, Gardiner, NY). This process was carefully monitored by regularly sampling the homogenate and viewing the myofibrils by phase contrast microscopy (40×). After the muscle had been homogenized and optimally diluted, 4–5 drops were applied to cold coverslips, incubated for 20 min, fixed 10 min in fresh 4% paraformaldehyde in PBS, and stored at 4°C in PBS + 0.02% sodium azide.

Immunofluorescence and microscopy

For isolated myofibrils, immunofluorescence staining was performed as described previously (5). Briefly, coverslips with adherent, fixed myofibrils were blocked in 3% bovine serum albumin/PBS and 1–3% normal goat serum for 20 min to decrease nonspecific staining. Coverslips were then incubated for 45 min with primary antibodies. Secondary antibodies, mixed with phalloidin, were incubated for 30 min. A 30–45-min wash in PBS followed each incubation. Coverslips were mounted onto glass slides using ProLong Gold (Molecular Probes) antifade reagent. All isolated myofibril images (0.10532 μm/pixel) were acquired on an Applied Precision (Issaquah, WA) Deltavision-RT System with SoftWorx software, using an Olympus (Tokyo, Japan) IX-71 microscope, a 60×/1.42 NA PlanApoN objective lens, and a Photometrics (Tuscon, AZ) CoolSnapHQ CCD camera. Raw images (i.e., not deconvolved images) were analyzed with a custom-designed distributed deconvolution plugin for ImageJ (31) (see Fig. S2).

For cryosectioned muscle fibers mounted on glass slides, immunofluorescence staining, similar to staining on the isolated myofibrils, was performed, except that larger volumes and longer times for the staining and washing steps were used for the cryosectioned muscle fibers. Briefly, sections were hydrated 15 min in PBS containing 0.1% Triton-X 100 (PSBT), permeabilized 30 min in PBS with 0.3% Triton, and blocked for 2 hr in blocking buffer (3% bovine serum albumin and 1% normal goat serum in PBST). Blocked samples were incubated in a humid chamber overnight at 4°C with 150 μl of primary antibody mixture against either Tmod/α-actinin or NebN/α-actinin prepared in blocking buffer. Samples were incubated in a humid chamber for 2 hr at 25°C with 150 μl of the secondary antibody mixture containing phalloidin prepared in blocking buffer. Antibody mixtures were spread by laying a 60 × 22-mm coverslip over all the sections, with care taken to prevent bubbles. After each antibody incubation, the coverslip was removed by dipping the slide in PSB, and the slides were washed 3 × 20 min in PBST at 25°C. Coverslips were mounted on the stained sections in Gel/Mount (Biomeda, Foster City, CA) and sealed with clear nail polish. All cryosection images were acquired with a Bio-Rad (Hercules, CA) Radiance 2000 Confocal on a Nikon (Tokyo, Japan) E800 microscope with a Plan Apo 60×/1.40 NA objective lens at 3× zoom. The pixel size (0.0658 μm/pixel) was determined using a stage micrometer. Tmod and NebN images were collected with an iris size of 1.5 mm for optimal confocality with 488 nm excitation.

RESULTS

To determine nebulin and thin filament lengths, we co-stained myofibrils from seven different rabbit muscles with fluorescently labeled phalloidin (Fig. 1, *A* and *B*; *green*) and with antibodies specific either for Tmod (Fig. 1 *A*, *red*), or for the first three N-terminal modules (M1–3) of nebulin

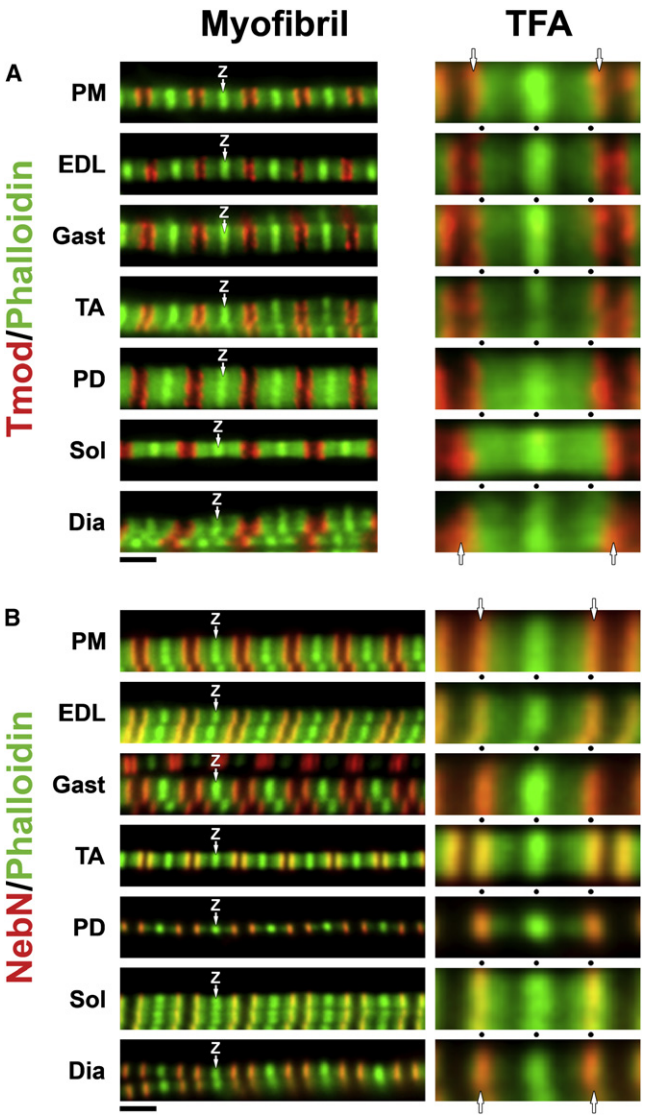

FIGURE 1 Rabbit skeletal myofibrils co-stained for actin (phalloidin, *green*) and either Tmod (*A*, *red*) or NebN (*B*, *red*). *Z*, Z-lines; Scale bars, 2 μm. Individual thin filament arrays (*TFA*) within myofibrils are at 3× magnification and aligned at the Z-line. Alignment guides (*black dots*) indicate 1 μm intervals. Arrows denote NebN and Tmod striations. NebN striations appear as different colors, because the degree of overlap between phalloidin and the NebN epitopes varies within the different muscles and because phalloidin staining along the thin filament lengths varies relative to Z-lines.

(NebN) (6) (Fig. 1 *B*, *red*). In all muscles, phalloidin stained along the lengths of the thin filaments, often appearing as wide bands with a central bright striation at the Z-line due to barbed-end overlap (Fig. 1, *A* and *B*; *Z*). However, varying degrees of nonuniform phalloidin staining along the length of the thin filament were also observed, likely resulting from binding inhibition by nebulin (9,32,33). In stretched myofibrils, a gap in phalloidin staining (H-zone) was visible in the middle of each sarcomere. The presence of H-zones (and Tmod doublets, see below) indicated that thin filament lengths are precisely specified in these muscles. However, because nonuniform phalloidin staining tended to interfere with distributed deconvolution analysis, we relied instead on the location of Tmod to investigate the position of the P-ends with respect to the position of the NebN epitopes.

As expected, Tmod (Fig. 1 *A*, *red*) localized to closely spaced doublets in stretched myofibrils at the extreme edges of the wide phalloidin bands (5,7,10,34). Based on a visual examination of the individual thin filament arrays (TFA) within different muscles (Fig. 1 *A*, *TFA*), Tmod striations were located at slightly different positions from Z-lines: closest in psoas major (*PM*), extensor digitorum longus (*EDL*), tibialis anterior (*TA*), and gastrocnemius (*Gast*) myofibrils, intermediate in pectoralis descendens (*PD*), and furthest in soleus (*Sol*), and diaphragm (*Dia*) myofibrils. Using distributed deconvolution image analysis, we quantified the distance between Tmod striations and Z-lines in the seven muscles (Table 1, Tmod length parameters). Average Tmod lengths ranged from 1.13–1.31 μm among the seven muscles with PM < EDL, Gast, and TA < PD < Sol and Dia, confirming the trend observed by visual inspection. Based on the consistent localization of Tmod at the end of the phalloidin bands in each TFA (Fig. 1 *A*), the biochemical actin P-end-capping activity of Tmod in vitro, and the localization of Tmod at the thin filament P-ends in other muscles (5,7), we interpreted Tmod length to be a precise and accurate determinant of thin filament lengths. In particular, the average Tmod length for PM (1.13 $\pm$ 0.03 μm; n = 248 linescans) agreed well with previous thin filament length measurements of 1.12 μm (27), 1.11–1.15 μm (28), 1.12 μm (1), and 1.16 μm (35), from both electron and light microscopy approaches.

The NebN antibody specifically stained narrow, double striations (doublets) (Fig. 1 *B*, *red*) in the middle of each sarcomere. In stretched myofibrils with a visible H-zone (i.e., a gap in phalloidin staining), we observed only NebN doublets consistent with an association close to thin filament P-ends. However, closely spaced NebN doublets or single striations (singlets) were occasionally observed in some PD, Sol and Dia myofibrils when an H-zone was not visible (A. Castillo, R. Nowak, K. P. Littlefield, V. M. Fowler, and R. S. Littlefield, unpublished data). Individual TFAs of isolated myofibrils from each muscle were aligned at Z-lines to compare NebN localization (Fig. 1 *B*, *TFA*). Among the different muscles, there was no observable variation in the NebN epitope locations with respect to the Z-line. However, in PD, Sol, and Dia myofibrils, phalloidin staining often extended beyond the NebN epitope (Fig. 1 *B*). Using distributed deconvolution analysis, we measured the distance between the NebN epitope and the Z-line in each of the seven muscles (Table 1, NebN length parameters). NebN lengths were extremely uniform between different myofibrils, muscles, and rabbits, consistent with C-terminal anchoring at the Z-line. Average NebN lengths ranged between 1.01 and 1.03 μm and were not significantly different among all seven muscles.

For all seven muscles, average Tmod lengths were significantly greater than average NebN lengths (Table 1, ΔL).

TABLE 1 Rabbit NebN and Tmod length parameters determined by distributed deconvolution

	NebN length parameters (μm)		Tmod length parameters (μm)		Tmod-NebN			NebN SL (μm)	Tmod SL (μm)
Muscle	Ave ± SD	*n*	Ave ± SD	*n*	ΔL (nm)	*P*-value	LCV (nm)	Min–Max	Min–Max
PM	1.03 ± 0.02	239	1.13 ± 0.03	248	106	0.0009	54	2.59–3.24	1.67–3.12
EDL	1.03 ± 0.04	104	1.16 ± 0.02	83	131	0.0049	96	1.66–2.88	1.91–3.18
Gast	1.02 ± 0.03	112	1.20 ± 0.07	200	182	0.0055	87	1.59–3.05	1.56–3.74
TA	1.02 ± 0.02	126	1.18 ± 0.03	262	159	1.9E–05	132	2.37–3.27	2.40–3.40
PD	1.03 ± 0.03	111	1.23 ± 0.07	103	203	0.0063	135	2.36–3.67	2.43–3.65
Sol	1.01 ± 0.06	130	1.27 ± 0.09	150	252	0.0092	138	2.38–3.56	2.65–3.55
Dia	1.03 ± 0.04	147	1.31 ± 0.08	126	290	1.3E–05	226	2.34–4.07	2.85–3.72

Ave, average; SD, standard deviation; *n*, number of linescans; ΔL, difference in length parameters (Tmod–NebN); *p*-value, probability that length parameters are equal (one-sided *t*-distribution); LCV, lower confidence value for ΔL ($p = 0.05$); PM, psoas major; EDL, extensor digitorum longus; Gast, gastrocnemius; TA, tibialis anterior; PD, pectoralis descendens; Sol, soleus; Dia, diaphragm. Minimum (min) and maximum (max) sarcomere lengths (SL) were determined for NebN and Tmod myofibrils.

Lower 95% confidence values (Table 1, 95% *LCV*) indicated that the thin filament P-ends extended beyond nebulin by at least 54–226 nm, depending on the muscle. Because NebN and Tmod images were analyzed using the same parameters (see the Supporting Material), this difference was not likely due to a systematic fitting error. In addition, for all rabbit muscles except for PM and EDL, the variation in Tmod lengths was significantly greater than the variation in NebN lengths, even among different myofibrils from the same rabbit (Table 1; Fig. 2; and A. Castillo, K. P. Littlefield, and R. S. Littlefield, unpublished data). This was unlikely due to measurement error since paired Tmod and phalloidin length measurements (i.e., from the same myofibril) were well-correlated (A. Castillo, K. P. Littlefield, and R. S. Littlefield, unpublished data). Instead, the variation in the Tmod lengths suggested that, in contrast to the NebN epitopes, the locations of the thin filament P-ends were not strictly determined by their distance from the Z-line. Collectively, average Tmod lengths ranged by ~170 nm, whereas NebN lengths ranged by ~30 nm among all the muscles (Fig. 2; Table 1). Importantly, the Tmod and NebN length distributions were incompatible with a ruler mechanism where nebulin binds Tmod to specify thin filament length.

To exclude any possible artifacts from the image analysis, we sought to directly colocalize Tmod and NebN epitopes within the same myofibrils. We were unable to successfully co-stain rabbit myofibrils with the rabbit polyclonal antibodies to Tmod and NebN. Instead, we used a mouse monoclonal anti-Tmod antibody (mAb95) that recognized chicken (but not rabbit) myofibrils (5,34), to co-stain isolated myofibrils from chicken biventer (CBV) muscle for Tmod and NebN (see Supplemental Methods in the Supporting Material). In CBV myofibrils, both NebN and Tmod epitopes appeared as narrow doublets (Fig. 3 *A*) or singlets, similar to rabbit myofibrils. Merged images (Fig. 3 *A*, *merge*) and linescans (Fig. 3 *B*) of CBV myofibrils stained for NebN and Tmod showed that these epitopes did not colocalize, but were instead separated by >200 nm within the same sarcomere, consistent with the resolution of light microscopy. Using distributed deconvolution analysis, we found that the NebN and Tmod epitopes were 1.00 ± 0.04 μm and 1.27 ± 0.06 μm, respectively, from the Z-line ($n = 47$ myofibrils). Pairwise differences for each co-stained myofibril showed that the Tmod epitope was located significantly further by 0.27 ± 0.07 μm (P = 1E-30; two-tailed paired *t*-test) from the Z-line than the NebN epitope (Fig. 3 *C*). Our measurements in CBV myofibrils confirm our results in rabbit myofibrils, and indicate that nebulin does not extend along the entire thin filament to the P-end where Tmod is located.

To investigate whether the positions of the Tmod and NebN epitopes were dependent on the method of myofibril preparation, we prepared and stained rabbit muscles for NebN and Tmod epitopes using two alternative methods. First, we prepared cryosections of relaxed rabbit muscle fibers from PM, PD, Sol, and Dia muscles that had been fixed in paraformaldehyde, and, second, we prepared isolated myofibrils from muscles extracted overnight with Triton X-100 (see the Materials and Methods section). As before, NebN and Tmod staining appeared as narrow doublet striations in moderately stretched regions of the cryosectioned fibers (Fig. 4 *A*; and R. Nowak, V. M. Fowler, and R. S. Littlefield, unpublished results) or in the Triton-extracted myofibrils (R. Nowak, K. P. Littlefield, V. M. Fowler, and R. S. Littlefield, unpublished results). Alignment and close inspection of the merged images showed that the NebN epitope (Fig. 4 *A*, *gold arrowheads*) was located closer to the Z-line than the Tmod epitope (Fig. 4 *A*, *red arrowheads*), as observed for glycerol-extracted myofibrils (Fig. 1). In addition, the wide phalloidin band extended away from the Z-line up to the Tmod epitope, consistent with its location at thin filament P-ends, but it extended past the NebN epitope, suggesting that nebulin did not extend along the entire length of the thin filaments (Fig. 4 *A*, *green arrowheads*). Myofibril linescans (Fig. 4 *B*) confirmed the appearance of the images. Using distributed deconvolution image analysis, we found that average position of the NebN epitope was 0.99–1.03 μm from the Z-line and the average position of the Tmod epitope was 1.19–1.29 μm from the Z-line (Fig. 4 *C* and Table S1). Similarly, for the Triton-extracted myofibrils, the average position of the NebN epitope was

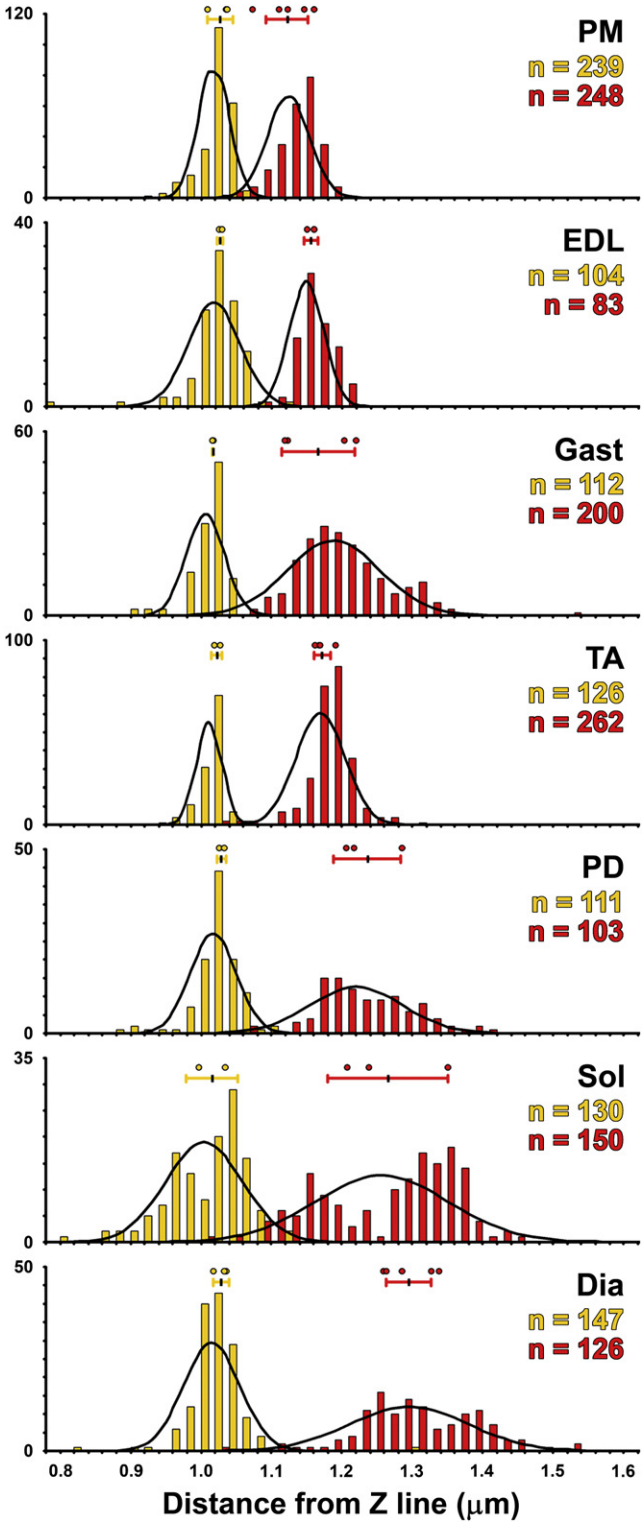

FIGURE 2 Nebulin and Tmod lengths determined by distributed deconvolution image analysis in glycerinated rabbit myofibrils. Each histogram reports the number of myofibrils observed (*y* axis) for Tmod (*red*) and NebN (*gold*) length parameters values (μm), binned at 20-nm intervals (*x* axis). Number of myofibril linescans for Tmod and NebN in each muscle (*n*) are listed in Table 1. Number of rabbits for NebN: Total, 4; PM, 3; EDL, 2; Gast, 2; TA, 2; PD, 2; Sol, 2; Dia, 3. Number of rabbits for Tmod: Total, 6; PM, 5; EDL, 2; Gast, 4; TA, 4; PD, 3; Sol, 3; Dia, 5. Normal distributions (*black lines*) show the expected number of observations for each probe. Circles denote average thin filament length determined for an individual rabbit. Horizontal bars indicate average thin filament length ± SE determined from all rabbits.

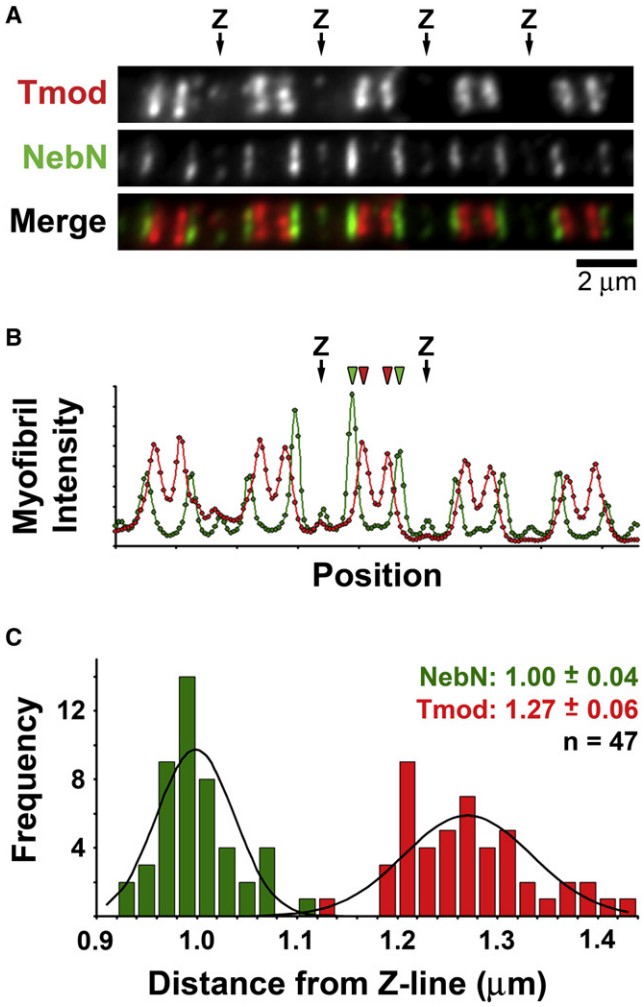

FIGURE 3 Tmod and NebN epitopes do not colocalize in chicken biventer muscle. (*A*) Chicken biventer myofibril co-stained for Tmod (*red*) and NebN (*green*). Tmod and NebN epitopes are distinctly resolved (*Merge*). Scale bar, 2 μm. (*B*) Myofibril intensity linescans of NebN (*green*) and Tmod (*red*) fluorescence. Arrows indicate position of Z-lines (*Z*); green and red arrowheads indicate position of NebN and Tmod epitopes, respectively. (*C*) Histogram of Tmod (*red*) and NebN (*green*) length parameters. Values are average ± SD; *n* is number of myofibrils. Black lines are expected normal distributions.

0.99–1.06 μm from the Z-line, whereas the average position of the Tmod epitope was 1.09–1.24 μm from the Z-line (Table S1). Thus, both alternative preparations showed significantly longer lengths for the Tmod epitope, compared to the NebN epitope, for all muscles, confirming our results for glycerinated myofibrils. Furthermore, the position of the NebN epitope was nearly identical for all muscle types, whereas the Tmod epitope varied in position, showing the

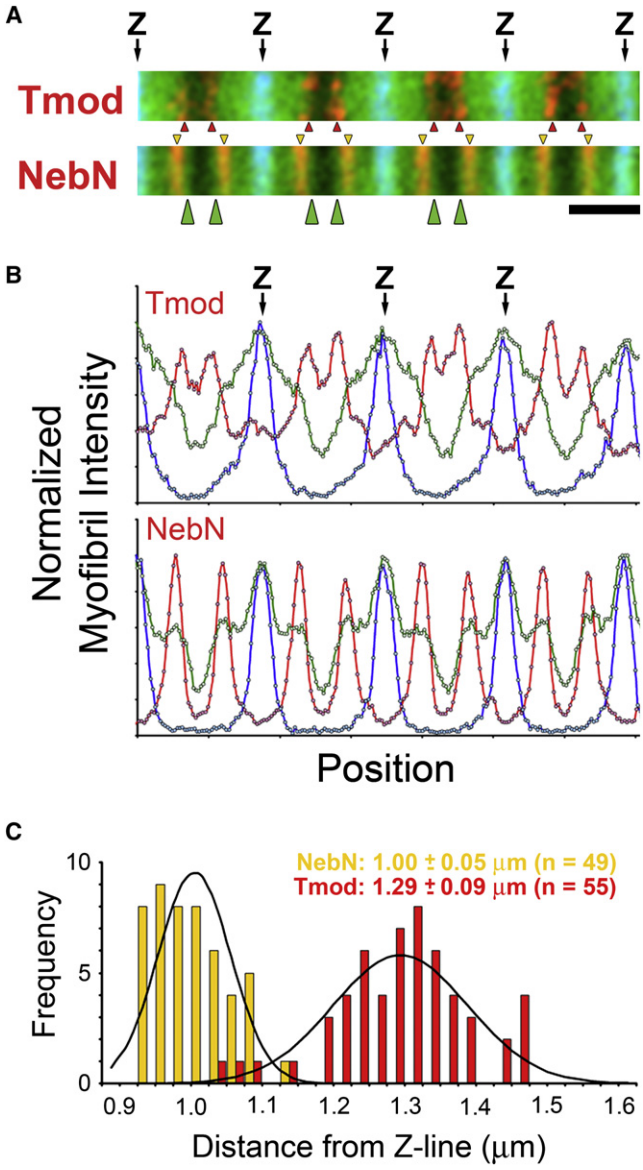

FIGURE 4 NebN domain does not colocalize with Tmod at the thin filament P-end in cryosections of rabbit Sol muscle fixed in situ. (*A*) Rabbit Sol myofibrils co-stained for either Tmod or NebN (*red*), F-actin (phalloidin, *green*), and α-actinin (*blue*). Arrows indicate position of Z-lines (*Z*). Red and gold arrowheads indicate Tmod and NebN striations, respectively. Green arrowheads indicate where phalloidin staining extends further from the Z-line than does the NebN epitopes. Scale bar, 2 μm. (*B*) Myofibril intensity linescans of myofibrils in *A*. (*C*). Histograms of NebN (*gold*) and Tmod (*red*) length parameters. Values are average ± SD; *n* is number of myofibrils. Black lines are expected normal distributions.

same general trend observed for glycerinated myofibrils. We conclude that the differences we observed between the NebN and Tmod epitope positions are not dependent on the method of myofibril preparation and are therefore likely to exist in vivo.

Because nebulin length did not account for variations in thin filament lengths within and between muscles, we asked whether this variation was correlated with any other architectural features of the sarcomere. Because of titin's known structural role in the sarcomere, we compared Tmod lengths with the titin isoform sizes expressed in these muscles (Fig. 5). Interestingly, we found that Tmod lengths correlated significantly with titin isoform size in rabbits ($r^2 = 0.92$; $p = 0.0006$). The regression coefficient indicated that Tmod lengths increased on average by 4.12 nm per 10 kD of titin size, consistent with titin being composed primarily of immunoglobulin and fibronectin domains (36) (see the Supporting Material). In addition, CBV muscle, which expresses a 3.7 MDa titin isoform (37), has a Tmod length (1.27 ± 0.06 μm) consistent with the relationship we found between titin sizes and thin filament lengths in rabbits (Fig. 5, *circle*). Because titin is believed to be the main determinant of resting sarcomere lengths (36,38), the regression between Tmod lengths and titin isoform sizes suggests that thick-thin filament overlap is physiologically optimal within all of these muscles and that thin filament lengths are coordinated with titin isoform size.

DISCUSSION

Our NebN length measurements place the NebN epitope further away from the Z-line than any other measured nebulin epitope, and they therefore contribute to mapping nebulin's layout within the sarcomere. Fig. 6 shows the layouts for nebulin in rabbit PM and rabbit Dia that are maximally consistent with the positions we determined for the NebN epitope as well as with other known epitope positions, estimated mol wts, available sequence data, and measured Z-line widths. In rabbit PM, 1–2 alternatively spliced modules present in the C-terminal region of nebulin (11) would result in a nebulin

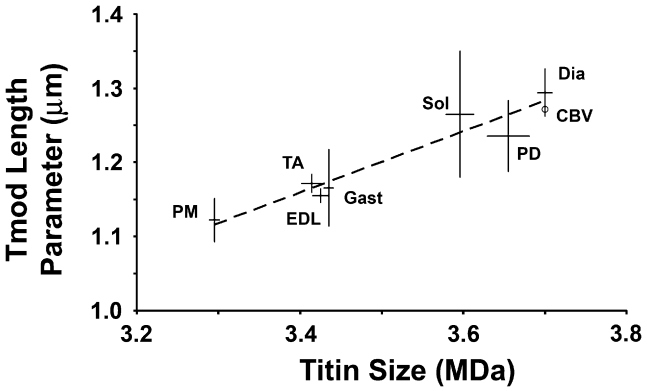

FIGURE 5 Tmod lengths vary in accordance with titin size. Titin size (MDa) versus Tmod length parameters (distance from Z-line, μm) were plotted for each muscle. Tmod lengths are mean ± SE of all rabbits. Titin isoform sizes (mean ± SE) are taken from Prado et al. (25). Dashed line, least-squares regression, $r^2 = 0.92$. Regression values (mean ± SE): slope, 4.12 ± 0.53 nm/10kD; *y*-intercept, −0.24 ± 0.19 μm. The slope is consistent with the expected sizes and masses of Fn3 and Ig domains in titin. The intercept suggests that ~0.59 MDa (= 0.24/0.41) of titin mass does not contribute to Tmod lengths. Circle represents chicken biventer (CBV) myofibrils.

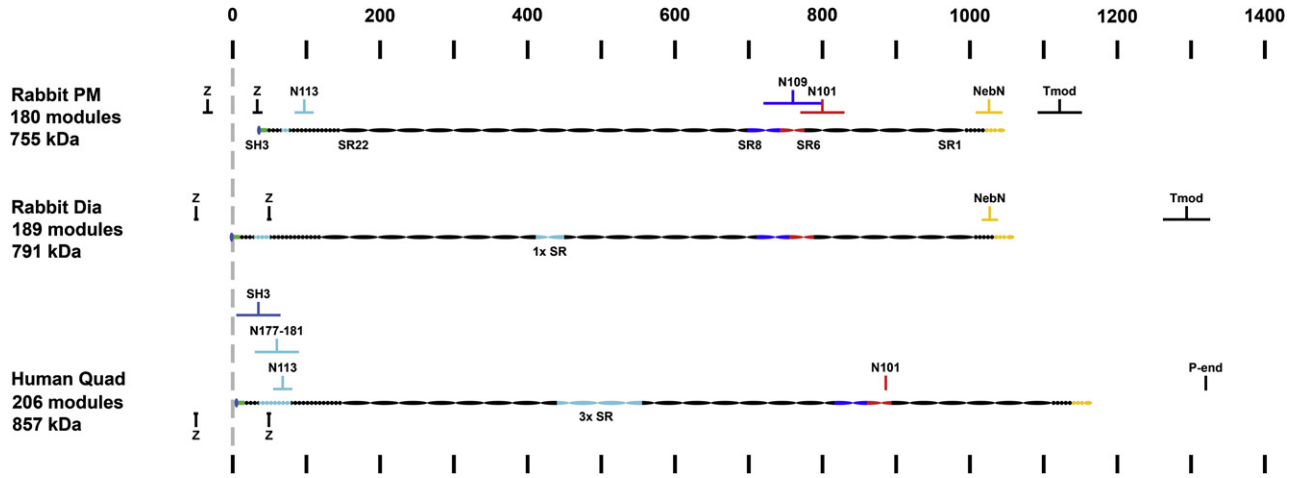

FIGURE 6 Predicted layout of nebulin within the sarcomere. Scale diagrams for nebulin isoforms in rabbit PM, rabbit Dia, and human quadriceps (*quad*). Circles denote individual nebulin modules, ovals denote nebulin super-repeats (seven modules). Alternatively expressed modules are shaded light blue. Epitope regions are shaded (*dark blue*, N109; *red*, N101; *yellow*, NebN). Mapped epitope locations relative to the Z-line are indicated by brackets. Epitopes to C-terminally expressed modules are shaded light blue. Black brackets: measured Tmod lengths for rabbit PM and Dia (Tmod), thin filament lengths in human gastrocnemius muscle (P-end), edges of Z-lines (*Z*). Dashed gray line, center of Z-line. Ruler indicates 100 nm distances from center of Z-line. Nebulin isoforms shown for rabbit Dia and human quadriceps contain one (1xSR) and three (3xSR) super-repeats.

isoform with 179–180 modules, having a mass of ~755 kDa consistent with mol wt estimates of 700–770 kDa (1,25) and extending at least 990 nm (5.5 nm per module), allowing it to extend from the edge of the Z-line (~66 nm wide) (11,26) to the NebN epitope located ~1030 nm from the Z-line center. This layout is consistent with the localization of polyclonal antibodies to nebulin up to ~1.0 μm from the Z-line (12), randomly generated nebulin monoclonal epitopes up to 0.85 μm from the Z-line (1), and site-specific monoclonal epitopes N101, N109, and N113 (13). In particular, modules S6R5–S7R4 of nebulin, located 748–780 nm from the Z-line in this layout, was localized 800 $\pm$ 30 nm from the Z-line with mAb N101 (13). Similar layouts (not shown) would be expected in rabbit Gast, EDL, TA, and PD muscles based on their similar mol wts (25), similar number of C-terminal modules (11), and similar positions of the NebN epitope. However, based on mol wt estimates of 770–820 kDa (1,25) and the presence of ~3–4 alternatively spliced single modules in their C-terminal regions (11), we suggest that rabbit Dia (Fig. 6) and Sol (not shown) nebulin isoforms would contain one additional super-repeat and have a mass of ~791 kDa. These isoforms would be expected to be ~49.5 nm longer than the PM nebulin isoform, but, because we did not observe any difference in the NebN epitope positions, they may extend further in toward the center of the ~100 nm wide Z-lines (26). Further epitope mapping and sequencing of nebulin isoforms will be necessary to refine these nebulin layouts in different muscles. In particular, immunoelectron microscopy approaches, with their inherent nanometer resolution, will likely be required to map nebulin epitopes near the Z-line and evaluate models proposed by Millevoi et al. (11) and by Pappas et al. (39) for ways in which nebulin may regulate Z-line width (22,23,40–42). Importantly, these nebulin layouts show that our measurements of NebN positions are consistent with all other available nebulin data in rabbits and suggest that nebulin is unlikely to extend further than ~1.05 μm from the Z-line.

Our localization and measurement of NebN and Tmod epitopes indicate that thin filaments extend past nebulin and are thus composed of nebulin-bound ''core regions'' and nebulin-free ''P-end extensions'' (Fig. 7). In co-stained CBV myofibrils, NebN and Tmod epitopes were separated by 270 $\pm$ 70 nm and were clearly resolved as distinct striations by light microscopy (Fig. 3). In rabbit muscles, where co-staining for NebN and Tmod was not possible, we inferred the presence of ~100–300 nm P-end extensions by visually comparing the positions of NebN and Tmod striations within separately stained myofibrils, by visually comparing NebN and Tmod striations with phalloidin co-staining, and by quantitative image analysis of NebN and Tmod for three different preparations, including fixed, intact tissue. The presence (i.e., nonzero length) of P-end extensions of actin can explain why nebulin does not inhibit phalloidin binding at P-ends in unfixed myofibrils (32,33). In support, we observed broader regions of phalloidin binding at the P-ends of unfixed Sol and Dia myofibrils relative to PM myofibrils, consistent with the size of their P-end extensions (A. Castillo, K. P. Littlefield, and R. S. Littlefield, unpublished results).

Based on the available literature, P-end extensions are likely to be present in other muscles and species. In particular, a human quadriceps (HQ) nebulin isoform (Fig. 6) containing seven alternatively expressed C-terminal modules and three alternatively expressed super-repeats (encoded, for example, by exons 82–93 (15)) would contain 206 modules and have a molecular mass of ~857 kDa, consistent with an

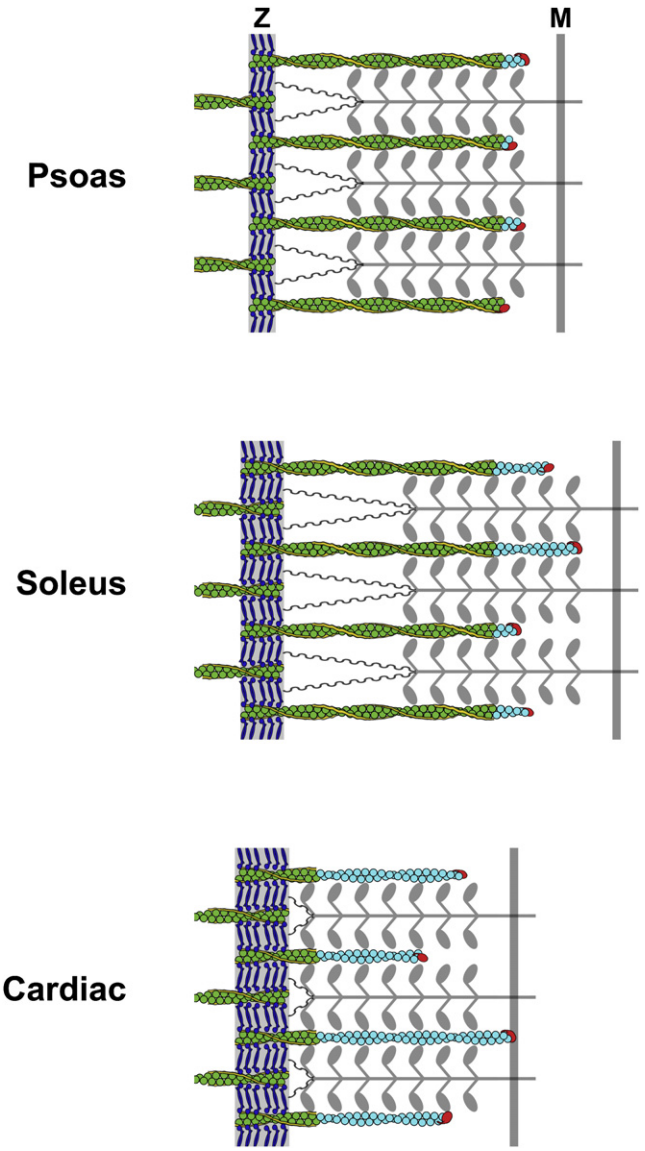

FIGURE 7 Schematic diagram of psoas, soleus, and cardiac half-sarcomeres. PM (psoas) muscle has intermediate titin I-band length (*gray wavy line*) and full-length, short nebulin (*yellow*), resulting in narrow Z-lines (*Z*), long, stable thin filament "core" regions (*green*) resistant to phalloidin binding, and short, dynamic actin P-end extensions that vary slightly in length (*light blue*). Tmod is indicated in red; alpha-actinin in dark blue. Sol (Soleus) muscle has a long titin I-band length and full-length, long nebulin, resulting in wide Z-lines (*Z*), long, stable thin filament "core" regions resistant to phalloidin binding, and intermediate, dynamic P-end extensions varying significantly in length. Cardiac muscle has short titin I-band length and short nebulette (*yellow*), resulting in wide Z-lines (*Z*), short thin filament "core" regions resistant to phalloidin binding, and large, dynamic P-end extensions varying broadly in length. The size of the P-end length extensions increase the overlap between thin and thick filaments (*gray*) to match resting half-sarcomere lengths in the different muscles, i.e., the distance between Z-line and M-line (*M*). Nebulin may partially extend through PM Z-lines and fully extend through sol Z-lines. For clarity, the tropomyosin/troponin strands are not shown.

estimated mol wt of 890 kDa (1). This HQ nebulin isoform, anchored with the C-terminal end within the Z-line, would be consistent with the positions previously determined for the SH3 domain and modules M177–181 (11), as well as for the N113 and N101 epitopes (13). Importantly, based on N101 epitope position (13) and the lack of alternative exons between this epitope and the N-terminus (15), nebulin would only extend ~1.14 μm from the Z-line. This is significantly less than the expected thin filament length of 1.32 μm (1), suggesting that P-end extensions may be ~180 nm in HQ muscle. Similarly, we calculate, using published immunoelectron micrographs, that the NebN epitope is located ~1.0 μm from the Z-line in mouse quadriceps, ~200 nm less than the thin filament length as determined by published fluorescence micrographs (see Fig. 4, *A* and *E*, in Witt et al. (23)). Furthermore, the correlation between nebulin isoform size and thin filament lengths observed by Kruger et al (1), although mainly interpreted to support the nebulin ruler mechanism, is structurally more consistent with the known dimensions of nebulin modules if the thin filaments have ~100-nm-long P-ends extensions (Fig. S3). In contrast to our results, Tmod and NebN epitopes were reported to colocalize in cultured skeletal myotubes (6); however, small P-end extensions (<100 nm) may have been undetected in this study without the use of distributed deconvolution to measure thin filament lengths.

This study provides important data for evaluating candidate mechanisms for regulating thin filament lengths. By showing that thin filaments P-ends extend beyond and vary independently of nebulin, our study excludes the proposed "ruler" function for nebulin. However, we observed that the minimum Tmod lengths closely coincided with the measured NebN lengths in each muscle (Figs. 2 and 3 *C*), suggesting that nebulin may, by preventing depolymerization (43) and stabilizing the thin filament core region, effectively define a minimum thin filament length. Interestingly, cardiac muscle thin filaments, which contain nebulette (21) are composed of short (nebulette) core regions and long P-end extensions with a broad length distribution (20). By respectively stabilizing large and small core regions, nebulin and nebulette may contribute to the narrow and broad thin filament length distributions found in skeletal and cardiac muscle (Fig. 7). Thus, our results indicate a previously unrecognized relationship between skeletal and cardiac muscle architecture and suggest that nebulin and nebulette, although structurally diverse, could have homologous stabilizing functions that may regulate the uniformity of thin filament lengths in vertebrate muscles.

This study further indicates that the thin filaments (and the P-end extensions) are regulated in length independently of nebulin. Indeed, the diverse thin filament lengths (1.13–1.31 μm) we observed in different muscles result primarily from the ~100–300 nm variation in lengths of the P-end extensions, and not from variations in nebulin isoform size or the lengths of the core region (Fig. 2). Furthermore, within single muscles (rabbit soleus), we observed significant greater variations (~100–200 nm) in Tmod lengths (Fig. 2) than in the position of NebN epitopes. This is similar to length variations observed in chicken muscles (Fig. 3 *C*) (5) and suggests that

thin filament lengths are not precisely determined by a molecular ruler, but may instead slightly vary due to dynamic Tmod capping and exchange of actin at P-ends (9). Nevertheless, the correlation we observed between thin filament lengths and titin isoform sizes in different muscles (Fig. 5) suggests that the lengths of the P-end extensions remain regulated and are unlikely to result from stochastic (unregulated) P-end dynamics (17). Our results therefore suggest that a nebulin-independent mechanism specifies thin filament lengths, likely by regulating the dynamics of P-ends and coordinating thin filament lengths with titin isoform sizes. This is reminiscent of *Drosophila* indirect flight muscle, which do not contain nebulin and in which the dynamics of thin filament P-ends are coordinated with sarcomere lengths during myofibril assembly, thereby preserving thin-thick filament overlap during sarcomere growth (18,19). In vertebrates, a nebulin-independent mechanism was recently found to be capable of specifying uniform thin filament lengths in nebulin-deficient mice at birth (22). However, our data suggest for the first time, to our knowledge, that this nebulin-independent mechanism actively specifies thin filament lengths in the presence of nebulin by extending the P-ends beyond a minimum length set by nebulin.

To account for optimal thin-thick filament overlap in different muscle types, we previously proposed that thin-thick filament interactions may regulate P-end dynamics independent of nebulin and effectively target P-ends to the edge of the thick filament bare zone (24). This type of mechanism is consistent with the correlation we observed between thin filament lengths and titin isoform sizes in different muscles; however, we cannot rule out other mechanisms that coordinate thin filament length and titin isoform size. We therefore favor a novel ''bipartisan'' mechanism (Fig. 7), where nebulin, by specifying minimum thin filament lengths, and a nebulin-independent mechanism, by modulating the lengths of P-end extensions and coordinating them with sarcomere length, could act in concert (44) to generate a variety of thin filament length distributions that are functionally optimized for the contractile properties of different muscles (45,46). Our approach using distributed deconvolution will benefit future studies that evaluate the structural consequences of naturally occurring or genetically engineered protein mutations in striated myofibrils.

SUPPORTING MATERIAL

Supplemental methods describe the estimation of nebulin repeats and molecular weights and image analysis details. Three supplemental figures describe the characterization of rabbit nebulin based on available genomic DNA sequences, distributed deconvolution modeling, and the correlation between nebulin isoform size and thin filament lengths from our data and from Kruger et al (1). Table S1 reports the NebN and Tmod lengths determined by distributed deconvolution image analysis for cryosectioned and Triton-extracted rabbit muscles. Table S2 lists the myofibril structural parameters used for nebulin conversions. A list of supplemental references is included. These are available at http://www.biophysj.org/biophysj/supplemental/S0006-3495(08)02331-X.

We gratefully acknowledge Dr. Carol Gregorio (University of Arizona, Tucson, AZ) for her generous gift of the NebN antibody. We thank Ryan Gile, Stephanie Palacio, and Madrona Murphy for assistance with dissections, Drs. Wolfgang Linke and Katarina Pelin for helpful discussions and sharing data, and Drs. Bob Fischer and Marie-Louise Bang for editorial suggestions.

R.S.L. and K.P.L. are supported by the National Institute of General Medical Sciences (P50 GM006605), and A.C. was supported by Friday Harbor Laboratories through a Blinks Fellowship for minority students.

REFERENCES

1. Kruger, M., J. Wright, and K. Wang. 1991. Nebulin as a length regulator of thin filaments of vertebrate skeletal muscles: correlation of thin filament length, nebulin size, and epitope profile. *J. Cell Biol.* 115:97–107.
2. Fowler, V. M., C. R. McKeown, and R. S. Fischer. 2006. Nebulin: does it measure up as a ruler? Curr. Biol. 16:R18–R20.
3. Kazmierski, S. T., P. B. Antin, C. C. Witt, N. Huebner, A. S. McElhinny, et al. 2003. The complete mouse nebulin gene sequence and the identification of cardiac nebulin. *J. Mol. Biol.* 328:835–846.
4. McElhinny, A. S., S. T. Kazmierski, S. Labeit, and C. C. Gregorio. 2003. Nebulin: the nebulous, multifunctional giant of striated muscle. *Trends Cardiovasc. Med.* 13:195–201.
5. Littlefield, R., and V. M. Fowler. 2002. Measurement of thin filament lengths by distributed deconvolution analysis of fluorescence images. *Biophys. J.* 82:2548–2564.
6. McElhinny, A. S., B. Kolmerer, V. M. Fowler, S. Labeit, and C. C. Gregorio. 2001. The N-terminal end of nebulin interacts with tropomodulin at the pointed ends of the thin filaments. *J. Biol. Chem.* 276:583–592.
7. Fowler, V. M., M. A. Sussmann, P. G. Miller, B. E. Flucher, and M. P. Daniels. 1993. Tropomodulin is associated with the free (pointed) ends of the thin filaments in rat skeletal muscle. *J. Cell Biol.* 120:411–420.
8. Weber, A., C. R. Pennise, G. G. Babcock, and V. M. Fowler. 1994. Tropomodulin caps the pointed ends of actin filaments. *J. Cell Biol.* 127:1627–1635.
9. Littlefield, R., A. Almenar-Queralt, and V. M. Fowler. 2001. Actin dynamics at pointed ends regulates thin filament length in striated muscle. *Nat. Cell Biol.* 3:544–551.
10. Gregorio, C. C., and V. M. Fowler. 1995. Mechanisms of thin filament assembly in embryonic chick cardiac myocytes: tropomodulin requires tropomyosin for assembly. *J. Cell Biol.* 129:683–695.
11. Millevoi, S., K. Trombitas, B. Kolmerer, S. Kostin, J. Schaper, et al. 1998. Characterization of nebulette and nebulin and emerging concepts of their roles for vertebrate Z-discs. *J. Mol. Biol.* 282:111–123.
12. Wang, K., and J. Wright. 1988. Architecture of the sarcomere matrix of skeletal muscle: immunoelectron microscopic evidence that suggests a set of parallel inextensible nebulin filaments anchored at the Z line. *J. Cell Biol.* 107:2199–2212.
13. Wright, J., Q. Q. Huang, and K. Wang. 1993. Nebulin is a full-length template of actin filaments in the skeletal muscle sarcomere: an immunoelectron microscopic study of its orientation and span with site-specific monoclonal antibodies. *J. Muscle Res. Cell Motil.* 14:476–483.
14. Labeit, S., T. Gibson, A. Lakey, K. Leonard, M. Zeviani, et al. 1991. Evidence that nebulin is a protein-ruler in muscle thin filaments. *FEBS Lett.* 282:313–316.
15. Donner, K., M. Sandbacka, V. L. Lehtokari, C. Wallgren-Pettersson, and K. Pelin. 2004. Complete genomic structure of the human nebulin gene and identification of alternatively spliced transcripts. *Eur. J. Hum. Genet.* 12:744–751.
16. Labeit, S., and B. Kolmerer. 1995. The complete primary structure of human nebulin and its correlation to muscle structure. *J. Mol. Biol.* 248:308–315.
17. Marshall, W. F. 2004. Cellular length control systems. *Annu. Rev. Cell Dev. Biol.* 20:677–693.

18. Mardahl-Dumesnil, M., and V. M. Fowler. 2001. Thin filaments elongate from their pointed ends during myofibril assembly in Drosophila indirect flight muscle. *J. Cell Biol.* 155:1043–1053.

19. Reedy, M. C., and C. Beall. 1993. Ultrastructure of developing flight muscle in Drosophila. I. Assembly of myofibrils. *Dev. Biol.* 160: 443–465.

20. Robinson, T. F., and S. Winegrad. 1977. Variation of thin filament length in heart muscles. *Nature.* 267:74–75.

21. Moncman, C. L., and K. Wang. 1995. Nebulette: a 107 kD nebulin-like protein in cardiac muscle. *Cell Motil. Cytoskeleton.* 32:205–225.

22. Bang, M. L., X. Li, R. Littlefield, S. Bremner, A. Thor, et al. 2006. Nebulin-deficient mice exhibit shorter thin filament lengths and reduced contractile function in skeletal muscle. *J. Cell Biol.* 173:905–916.

23. Witt, C. C., C. Burkart, D. Labeit, M. McNabb, Y. Wu, et al. 2006. Nebulin regulates thin filament length, contractility, and Z-disk structure in vivo. *EMBO J.* 25:3843–3855.

24. Littlefield, R., and V. M. Fowler. 1998. Defining actin filament length in striated muscle: rulers and caps or dynamic stability? Annu. Rev. Cell Dev. Biol. 14:487–525.

25. Prado, L. G., I. Makarenko, C. Andresen, M. Kruger, C. A. Opitz, et al. 2005. Isoform diversity of giant proteins in relation to passive and active contractile properties of rabbit skeletal muscles. *J. Gen. Physiol.* 126:461–480.

26. Schachat, F. H., A. C. Canine, M. M. Briggs, and M. C. Reedy. 1985. The presence of two skeletal muscle alpha-actinins correlates with troponin-tropomyosin expression and Z-line width. *J. Cell Biol.* 101:1001–1008.

27. Page, S. G., and H. E. Huxley. 1963. Filament lengths in striated muscle. *J. Cell Biol.* 19:369–390.

28. Sosa, H., D. Popp, G. Ouyang, and H. E. Huxley. 1994. Ultrastructure of skeletal muscle fibers studied by a plunge quick freezing method: myofilament lengths. *Biophys. J.* 67:283–292.

29. Hiraoka, Y., J. W. Sedat, and D. A. Agard. 1990. Determination of three-dimensional imaging properties of a light microscope system. Partial confocal behavior in epifluorescence microscopy. *Biophys. J.* 57:325–333.

30. Betzig, E., G. H. Patterson, R. Sougrat, O. W. Lindwasser, S. Olenych, et al. 2006. Imaging intracellular fluorescent proteins at nanometer resolution. *Science.* 313:1642–1645.

31. Rasband, W. S. 1997–2006. ImageJ. National Institutes of Health, Bethesda, MD.

32. Ao, X., and S. S. Lehrer. 1995. Phalloidin unzips nebulin from thin filaments in skeletal myofibrils. *J. Cell Sci.* 108:3397–3403.

33. Zhukarev, V., J. M. Sanger, J. W. Sanger, Y. E. Goldman, and H. Shuman. 1997. Distribution and orientation of rhodamine-phalloidin bound to thin filaments in skeletal and cardiac myofibrils. *Cell Motil. Cytoskeleton.* 37:363–377.

34. Almenar-Queralt, A., C. C. Gregorio, and V. M. Fowler. 1999. Tropomodulin assembles early in myofibrillogenesis in chick skeletal muscle: evidence that thin filaments rearrange to form striated myofibrils. *J. Cell Sci.* 112:1111–1123.

35. Ringkob, T. P., D. R. Swartz, and M. L. Greaser. 2004. Light microscopy and image analysis of thin filament lengths utilizing dual probes on beef, chicken, and rabbit myofibrils. *J. Anim. Sci.* 82: 1445–1453.

36. Labeit, S., and B. Kolmerer. 1995. Titins: giant proteins in charge of muscle ultrastructure and elasticity. *Science.* 270:293–296.

37. Granzier, H., M. Radke, J. Royal, Y. Wu, T. C. Irving, et al. 2007. Functional genomics of chicken, mouse, and human titin supports splice diversity as an important mechanism for regulating biomechanics of striated muscle. *Am. J. Physiol. Regul. Integr. Comp. Physiol.* 293:R557–R567.

38. Linke, W. A., M. Ivemeyer, N. Olivieri, B. Kolmerer, J. C. Ruegg, et al. 1996. Towards a molecular understanding of the elasticity of titin. *J. Mol. Biol.* 261:62–71.

39. Pappas, C. T., N. Bhattacharya, J. A. Cooper, and C. C. Gregorio. 2008. Nebulin interacts with CapZ and regulates thin filament architecture within the Z-disc. *Mol. Biol. Cell* 19:1837–1847.

40. Lehtokari, V. L., K. Pelin, M. Sandbacka, S. Ranta, K. Donner, et al. 2006. Identification of 45 novel mutations in the nebulin gene associated with autosomal recessive nemaline myopathy. *Hum. Mutat.* 27:946–956.

41. Wallgren-Pettersson, C., K. Donner, C. Sewry, E. Bijlsma, M. Lammens, et al. 2002. Mutations in the nebulin gene can cause severe congenital nemaline myopathy. *Neuromuscul. Disord.* 12:674–679.

42. Pelin, K., P. Hilpela, K. Donner, C. Sewry, P. A. Akkari, et al. 1999. Mutations in the nebulin gene associated with autosomal recessive nemaline myopathy. *Proc. Natl. Acad. Sci. USA.* 96:2305–2310.

43. Chen, M. J., C. L. Shih, and K. Wang. 1993. Nebulin as an actin zipper. A two-module nebulin fragment promotes actin nucleation and stabilizes actin filaments. *J. Biol. Chem.* 268:20327–20334.

44. Littlefield, R. S., and V. M. Fowler. 2008. Thin filament length regulation in striated muscle sarcomeres: pointed-end dynamics go beyond a nebulin ruler. *Semin. Cell Dev. Biol.* 19:511–519.

45. Granzier, H. L., H. A. Akster, and H. E. Ter Keurs. 1991. Effect of thin filament length on the force-sarcomere length relation of skeletal muscle. *Am. J. Physiol.* 260:C1060–C1070.

46. Rome, L. C. 2002. The design of vertebrate muscular systems: comparative and integrative approaches. *Clin. Orthop. Relat. Res.* 403 (Suppl.): S59–S76.